Measurement of Magnetic Field in Superconducting Undulators

Lee Teng Intern: Baichuan Huang[1]

Mentor: Matt Kasa[2]

[1] University of California, Berkeley
[2] Argonne National Laboratory

August 9, 2019

Abstract. Synchrotron radiation (SR), a kind of radiation produced when electrons travelling in a storage ring at a speed close to the speed of light, c, are radially accelerated, has been used in various fields of science. To create a high luminosity of synchrotron radiation, undulators are installed in storage rings, including the Advanced Photon Source (APS) at Argonne National Laboratory. Correspondingly, the measurement of magnetic field in an undulator, along with the subsequent determination of electron trajectory, slippage, phase error, and other quality factors, is essential to maintaining the efficiency of producing synchrotron radiation. This project aims to generate a LabVIEW program which analyzes the data of magnetic field measurement acquired in undulators in order to find electron trajectory and the quality factors mentioned above. This paper first discusses the mechanism of synchrotron radiation and undulators. It then explains the theoretical basis of this LabVIEW program that analyzes magnetic field measurement. An elaboration on the development and operation of this LabVIEW program is subsequently presented, as well as the results of this program when applied to the data of magnetic field measurement obtained in a superconducting undulator (SCU), a kind of undulator used in the ASD Division at Argonne. At last the paper summarizes the future plans to expand the utilities of this program.

Keywords: electron trajectory, LabVIEW, magnetic field, measurement, phase error, slippage, superconducting undulator, synchrotron radiation.

1 Introduction

By relativistic electromagnetic theory, when electrons travelling at a speed close to the speed of light, c, are radially accelerated, they lose a significant amount of energy by radiation, a process called *synchrotron radiation* (SR) [1]. Following scientists' discovery that synchrotron radiation can be efficiently used in various

fields such as solid-state physics, atomic physics, medicine and so on, a number of electron storage rings, including the Advanced Photon Source (APS) at Argonne National Laboratory, are installed to produce synchrotron radiation. In these storage rings, a series of magnets, *insertion devices*, are constructed and inserted into the accelerators so as to produce high levels of flux in a narrow region and thus act as powerful light sources.

One category of insertion devices used in APS is *undulator*, a device allowing electrons to follow a periodic and undulating trajectory in which SR waves interfere to create a high luminosity (Fig. 1). Our lab is currently developing superconducting undulator (SCU), a kind of undulator that produces strongly oscillating magnetic field thanks to the superconducting property, which can be later inserted into the updated APS storage ring (Fig. 2). In the development of SCU, measurement of magnetic field and subsequent calculations of electron trajectory, slippage and phase error are indispensable for verifying the design of SCU and for ensuring that the requirements of the storage ring and the users are met.

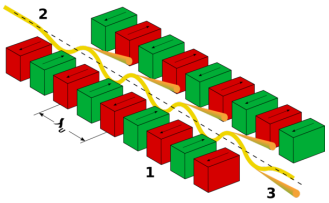

Fig. 1. Working of the undulator. [3] This device consists of periodic permanent dipole magnets (1). Electron beams (2) are injected into this undulator, where they undergo oscillations and produce synchrotron radiation (3).

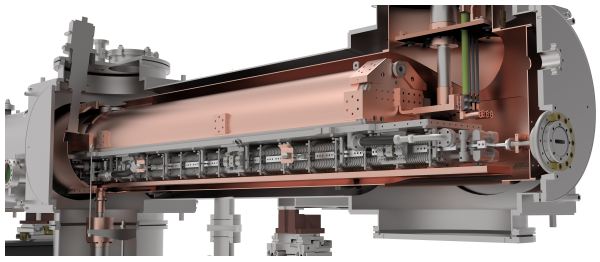

Fig. 2. Design Picture of an SCU. [4] This is a model of an SCU used in the ASD Division at Argonne National Laboratory. Instead of permanent magnets (Fig. 1), superconducting magnets are installed in a cryostat to produce a strongly oscillating magnetic field. Liquid helium is injected to create low temperature.

Correspondingly, the purpose of this project is to develop an algorithm to analyze the magnetic field measurement in SCU in order to find electron trajectory. After developing the integration routine to find electron trajectory, we generate further routines to find the quality factors of SCU that determine the intensity of synchrotron radiation.

2 Theoretical Basis

2.1 Electron Trajectory

Now we want to briefly demonstrate the theoretical basis of generating a LabVIEW program to calculate electron trajectory.[3]

Suppose that z is the direction of electron beam along the undulator, y is the upward direction, and x is determined by the right-hand coordinate system. Let $\gamma = \frac{1}{\sqrt{1-(v/c)^2}}$ be the Lorentz factor. Then, by Lorentz force equation, we have

$$\frac{\mathrm{d}}{\mathrm{d}t}v = \frac{q}{\gamma m}v \times B \tag{1}$$

In our coordinate system, (1) can be written as

$$\frac{\mathrm{d}}{\mathrm{d}t}v_x = -\frac{q}{\gamma m}v_z B_y \tag{2}$$

$$\frac{\mathrm{d}}{\mathrm{d}t}v_y = \frac{q}{\gamma m}v_z B_x \tag{3}$$

Now, since the electron is accelerated to a speed comparable to the speed of light, we have $v_z \gg v_x$ and $v_z \gg v_y$. Thus, we have $v_z = \frac{\mathrm{d}z}{\mathrm{d}t}$, so $\frac{\mathrm{d}}{\mathrm{d}t} = \frac{\mathrm{d}z}{\mathrm{d}t}\frac{\mathrm{d}}{\mathrm{d}z} = v_z\frac{\mathrm{d}}{\mathrm{d}z}$. Let the prime notation be the derivative with respect to z. Then, (2) and (3) can be written as

$$x'' = -\frac{q}{\gamma m v_z}B_y \tag{4}$$

$$y'' = \frac{q}{\gamma m v_z}B_x \tag{5}$$

Now we can work backwards to find the trajectory. Suppose that at the initial point $z = z_0$ the slope of the trajectory is 0. We integrate (4) and (5) to get the **slope** of electron trajectory:

$$x'(z) = \int_{z_0}^{z} x''(z_1)\mathrm{d}z_1 = -\frac{q}{\gamma m v_z}\int_{z_0}^{z} B_y(z_1)\mathrm{d}z_1 \tag{6}$$

$$y'(z) = \int_{z_0}^{z} y''(z_1)\mathrm{d}z_1 = \frac{q}{\gamma m v_z}\int_{z_0}^{z} B_x(z_1)\mathrm{d}z_1 \tag{7}$$

[3] This theoretical explanation is based on the discussion by Wolf, Z. [5]

We integrate (6) and (7) with respect to z again to get the **position** of electrons:

$$x(z) = \int_{z_0}^{z} x'(z_2)\mathrm{d}z_2 = -\frac{q}{\gamma m v_z}\int_{z_0}^{z}\int_{z_0}^{z_2} B_y(z_1)\mathrm{d}z_1\mathrm{d}z_2 \tag{8}$$

$$y(z) = \int_{z_0}^{z} y'(z_2)\mathrm{d}z_2 = \frac{q}{\gamma m v_z}\int_{z_0}^{z}\int_{z_0}^{z_2} B_x(z_1)\mathrm{d}z_1\mathrm{d}z_2 \tag{9}$$

Equations (6) $\sim$ (9) give us all the information about the trajectory of electrons, on which the calculations of quality factors of an undulator are based.

2.2 Slippage

In an undulator, the electron cannot keep up with the SR wave, which travels at the speed of light c. Also, alternating magnetic field in an undulator causes oscillation of electrons, which adds path length to electron trajectory. These two facts cause the electron to lag behind the SR wave. We define *slippage* to be the distance between a point on the SR wave and the electron. Slippage is thus a factor that determines the quality and efficiency of an undulator.

Suppose that SR wave travels at the speed of light c in the z direction and that the electron moves with speed v_z. Then, by the definition above, the slippage changes in a time interval dt by

$$dS = (c - v_z)dt \tag{10}$$

where S is slippage. Let us now use the parameter z, which denotes the position of a point on SR wave, to be the independent variable. Then, we have $dz = cdt$, so (10) can be rewritten as

$$dS = (1 - \frac{v_z}{c})dz \tag{11}$$

Now, a decomposition of the velocity of electron v gives

$$v^2 = v_z^2 + v_x^2 + v_y^2 \tag{12}$$

Using z as the independent variable, which corresponds with our stipulation above, we rewrite (12) as

$$v^2 = v_z^2\left(1 + \frac{v_x^2}{v_z^2} + \frac{v_y^2}{v_z^2}\right) = v_z^2[1 + x'(z)^2 + y'(z)^2] \tag{13}$$

By the definition of Lorentz factor,

$$\gamma = \frac{1}{\sqrt{1 - v^2/c^2}} \tag{14}$$

By (13) and (14),

$$v_z = c\frac{\sqrt{1 - \frac{1}{\gamma^2}}}{\sqrt{1 + x'(z)^2 + y'(z)^2}} \tag{15}$$

For electrons in undulators, we can assume $\frac{1}{\gamma^2} \ll 1$, $x'(z)^2 \ll 1$, and $y'(z)^2 \ll 1$. We can then apply the binomial approximation to get

$$v_z \approx c\left[1 - \frac{1}{2\gamma^2} - \frac{1}{2}x'(z)^2 - \frac{1}{2}y'(z)^2\right] \tag{16}$$

By (11) and (16), we get

$$dS = \left[\frac{1}{2\gamma^2} + \frac{1}{2}x'(z)^2 + \frac{1}{2}y'(z)^2\right]dz \tag{17}$$

Suppose that the initial slippage $S(z_0) = 0$. Integrating (17), we get the desired formula for **slippage**:

$$S(z) = \int_{z_0}^{z}\left[\frac{1}{2\gamma^2} + \frac{1}{2}x'(z_1)^2 + \frac{1}{2}y'(z_1)^2\right]dz_1 \tag{18}$$

3 Programming Methods: LabVIEW

Our goal now is to develop an algorithm to realize Equations (6) $\sim$ (9) and Equation (18), which respectively define the slope of electron trajectory, the position of electron, and the slippage. The algorithm is developed in LabVIEW, with the result of a LabVIEW VI that generates the above three parameters from the data of magnetic field measurement in an SCU.

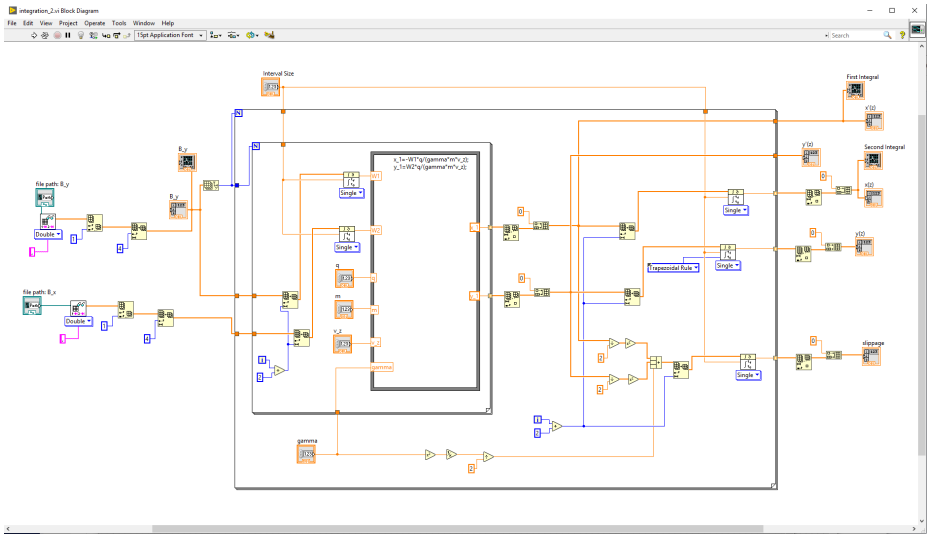

Fig. 3. Full block diagram of the VI.

Fig. 3 above is the full block diagram of this VI. For clarity we would like to explain the rationale of this VI within five parts.

3.1 Read Files

The VI first reads the CSV files containing the data of measurement of B_x and B_y in a superconducting undulator (Fig. 4). Two cropping VIs are inserted to extract the useful data from the CSV files. Those cropping VIs can be adjusted when another CSV file is analyzed where measurement data is contained in different rows or columns. In one branch of this part, the number of data is read and transported to the *count terminal* of the *for* loop (the integration step) later. In addition, *Array* VI and *Waveform Graph* VI can be inserted at the discretion of researchers to display the data of B_x and B_y.

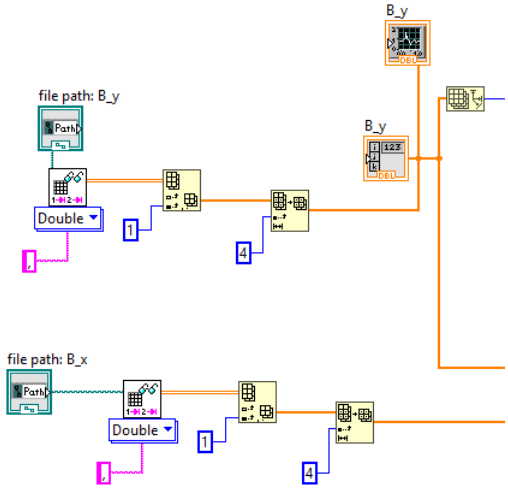

Fig. 4. Read-file section of the VI.

3.2 Looping Structure: Integration

After the read-file part, the data of B_x and B_y is transported in the form of arrays into the *for* loops (Fig. 5).

In the first *for* loop, two cropping VIs are applied separately to the arrays of B_x and B_y so as to correspond with the integration limits of Equation (6) and (7). Then we apply numeric integration VIs to realize these two equations, and the resultant arrays, now containing the first integral of B_x and B_y, are scaled in the *formula node*. The scaled arrays are our desired $x'(z)$ and $y'(z)$, which are transported out of the *for* loop for display in one pair of wires and are carried into the second loop for second integration in another pair. The scaling factors—the gamma factor γ, the mass of electron m, the charge of electron q, and the velocity of electron in z-direction—can be adjusted manually through the front panel according to the property of the electron beam in an undulator. In addition, the interval size of each numeric integration, which is identical to the interval of B_x or B_y in each scanning, can be adjusted through the front panel

as well. Note that we add a constant 2 to the *iteration terminal* $\boxed{\mathbf{i}}$ because the trapezoidal rule of numeric integration requires at least two data input. If the constant 2 is not added, the resultant array will have an NaN in its first element. Also note that after the arrays are carried out of this *for* loop, a *Delete from Array* VI is applied to each array because the $\boxed{\mathbf{i}}+2$ manipulation in the *for* loop causes the resultant array to produce the final element twice. We also append a constant element 0 at the beginning of each array because the $\boxed{\mathbf{i}}+2$ manipulation in the *for* loop starts at the second element of each array, which leaves out the initial value of the resultant array.

The arrays of $x'(z)$ and $y'(z)$ are now transported to the second *for* loop. In the top part of this loop, the arrays are cropped again to correspond with the integration limits of Equation (8) and (9). Then we apply numeric integration VIs to realize these two equations, and the resultant arrays, now containing $x(z)$ and $y(z)$, are carried out of the *for* loop for display. In the bottom part, some algebraic manipulations are applied to correspond with Equation (18). A similar numeric integration is applied to obtain the array of slippage; this array is then carried out of the loop for display as well.

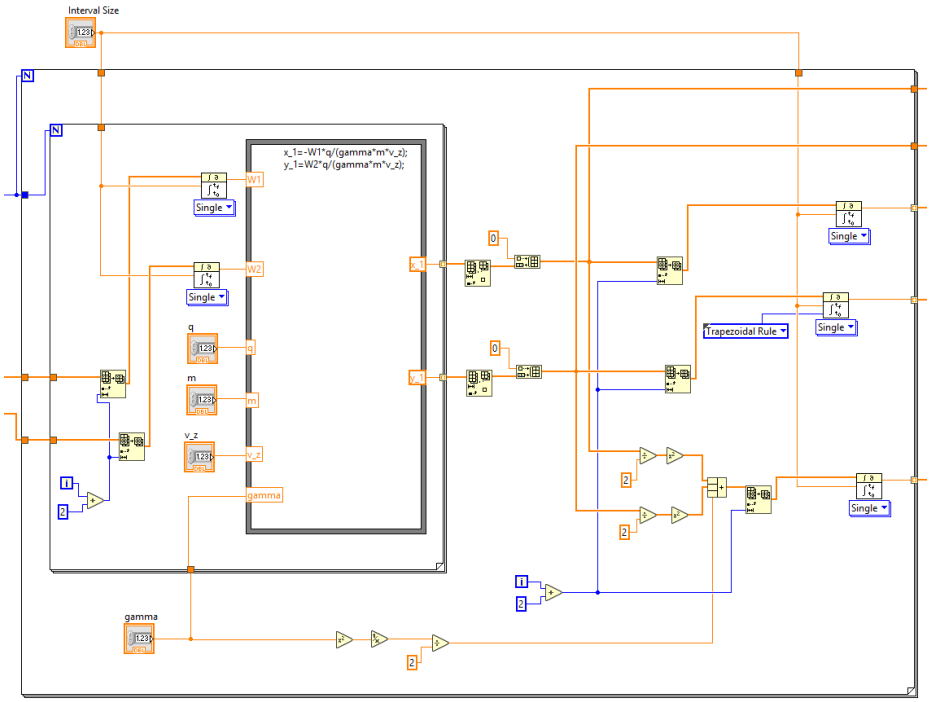

Fig. 5. Looping structure of the VI.

3.3 Display

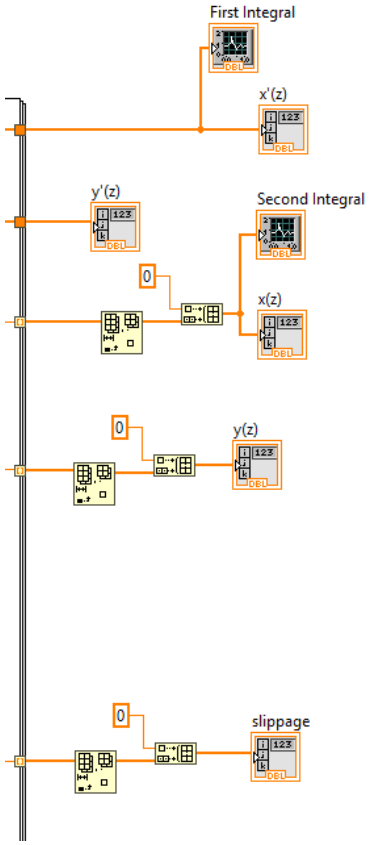

Fig. 6. Display section of the VI.

The arrays containing $x'(z)$, $y'(z)$, $x(z)$, $y(z)$, and the slippage are transported here for display (Fig. 6). Note that for the arrays of $x(z)$, $y(z)$ and the slippage we delete the last element and append a constant element 0 at the beginning due to the same reason as our previous manipulation with the arrays of $x'(z)$ and $y'(z)$ when they are carried out of the first *for* loop. After these operations, the arrays are displayed through *array indicators*. We may also wire a *Waveform Graph* terminal to each resultant array to visually display the desired parameters.

3.4 Front Panel

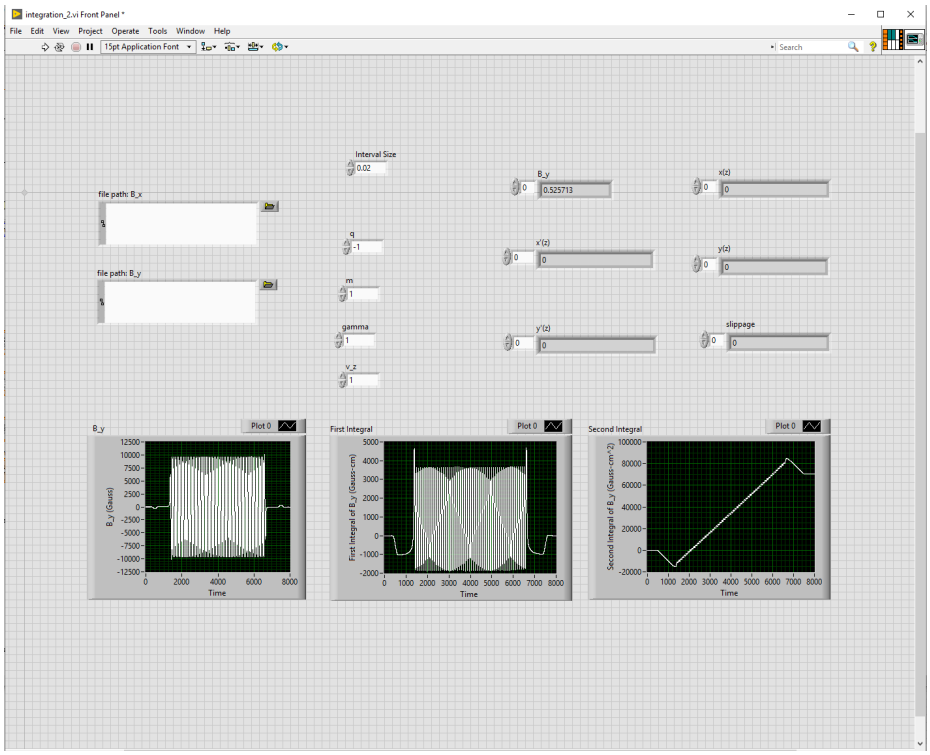

Fig. 7. Front Panel of the VI.

Fig. 7 shows the front panel of this VI. The scaling factors as well as the integration interval can be adjusted here through the numeric controls, and the resultant arrays are displayed both in array indicators and in waveform graphs. Note that this version of VI graphically displays B_y, the first integral of B_y, and the second integral of B_y. However, the other parameters, including the integrals of B_x and the slippage, can be displayed as well at the discretion of researchers: we simply need to switch to the block diagram and wire a *Waveform Graph* terminal to the array that we want to display.

3.5 subVI

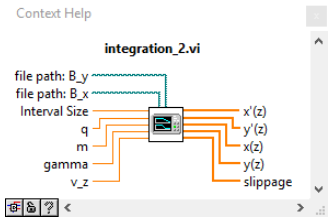

Fig. 8. A version of subVI.

Finally, we may pack all these features into a subVI. Fig. 8 shows one version of such subVI. The input consists of the file paths of B_x and B_y, the integration interval, and the scaling factors; we only need to wire appropriate constants to them. The outputs are array representations of $x'(z)$, $y'(z)$, $x(z)$, $y(z)$, and the slippage, but the graphic representations of them can be added to this subVI with minor changes in the block diagram and the assignment of subVI terminals. This subVI can be later incorporated into a larger VI or a project that analyzes the magnetic field measurement of undulators.

4 Results

The program is applied to a set of data obtained in the measurement of B_y of an SCU in the ASD Division at Argonne National Laboratory. From this data we can use this LabVIEW VI to plot B_y, which is shown in Fig. 9. The graph identifies with the strong oscillation of magnetic field in an SCU.

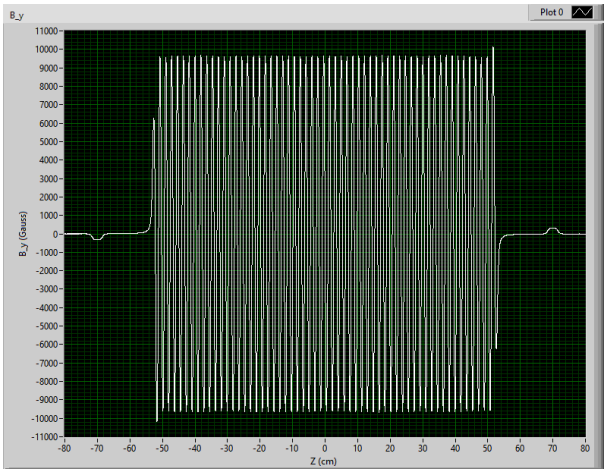

Fig. 9. A graph of B_y.

We use the VI to generate the first integral of B_y, which is plotted below in Fig. 10. The total scaling factor $-\frac{q}{\gamma m v_z}$ is set to 1. Note that we can adjust the scaling factors in the front panel according to the actual parameters in an SCU to obtain $x'(z)$. The graph identifies with the strong oscillation of the slope of electron trajectory in an SCU.

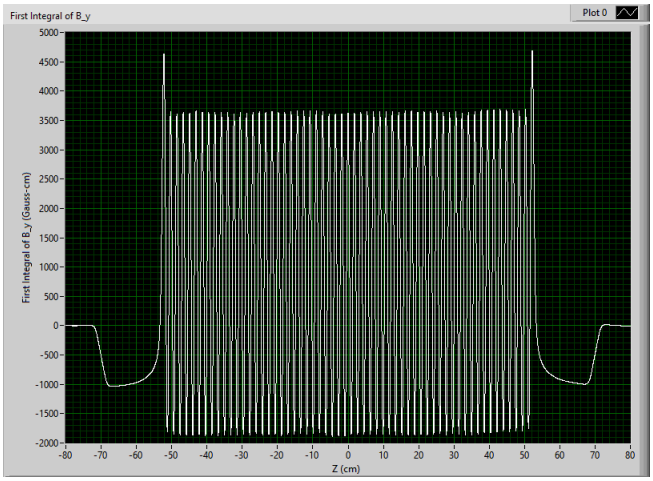

Fig. 10. The first integral of B_y. This graph is generated by the above LabVIEW VI.

We also use the VI to generate the second integral of B_y, which is plotted below in Fig. 11. Similar to the case of $x'(z)$, we can adjust the scaling factors in the front panel to obtain $x(z)$. The graph identifies with the expected trajectory of electrons in an SCU.

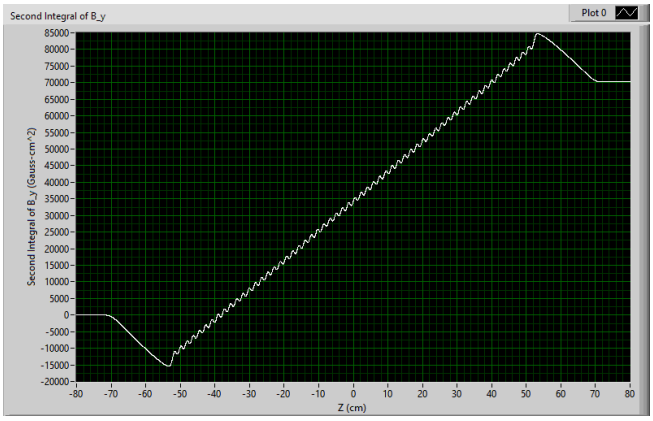

Fig. 11. The second integral of B_y. This graph is generated by the above LabVIEW VI.

To confirm the validity of this LabVIEW VI, we compare the above results with the results of a similar integration routine written in IDL, which is provided by Roger Dejus, a researcher in the PSC Division at Argonne National Laboratory. Graphs of first and second integrals of B_y using this earlier routine are shown below in Fig. 12 and Fig. 13, which identify with Fig. 10 and Fig. 11.

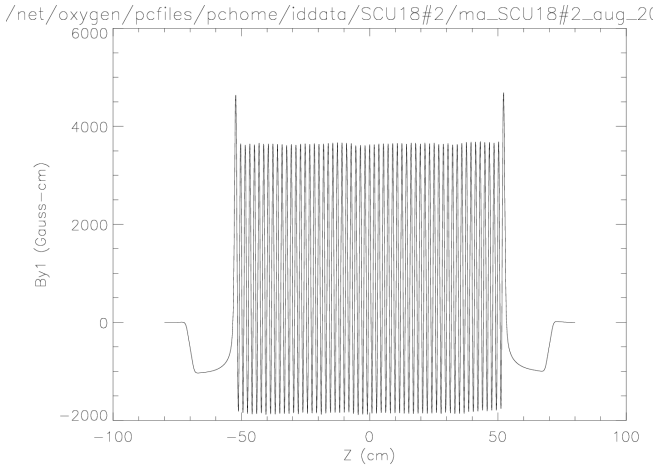

Fig. 12. The first integral of B_y. This graph is generated by IDL integration routine. [2]

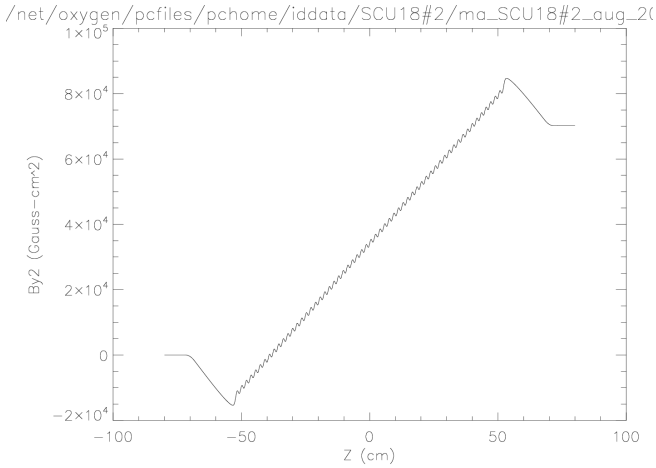

Fig. 13. The second integral of B_y. This graph is generated by IDL integration routine.[2]

We also compare several values of the first and second integrals of B_y generated by these two integration routines, which are shown in the tables below.

Index	LabVIEW 1st Integral (G-cm)	IDL 1st Integral (G-cm)	Relative Error (percent)
1389	4637.79	4638.70	0.020
1889	-1850.62	-1851.84	0.066
2383	3611.52	3612.52	0.028
2877	-1852.07	-1853.20	0.061
3371	3666.97	3668.16	0.032
3865	-1876.34	-1877.43	0.058
4359	3642.89	3643.86	0.027
4853	-1864.49	-1865.68	0.064
5347	3631.01	3632.16	0.032
5841	-1854.58	-1855.68	0.059
6334	3674.15	3675.22	0.029

Table 1. A comparison of several values of the first integral of B_y generated by the LabVIEW VI and the IDL routine. Note that the first column represents the index of elements in the two arrays.

Index	LabVIEW 2nd Integral (G-cm^2)	IDL 2nd Integral (G-cm^2)	Relative Error (percent)
604	-2177.21	-2177.24	1.4×10^{-3}
1043	-11022.8	-11022.86	5.4×10^{-4}
1425	-10977.4	-10976.98	3.8×10^{-3}
1923	-3242.24	-3242.76	1.6×10^{-2}
2462	6263.45	6262.90	8.8×10^{-3}
3020	17190.5	17190.70	1.2×10^{-3}
3641	28043.1	28042.98	4.3×10^{-4}
4259	38348.7	38348.11	1.5×10^{-3}
4942	51069.6	51069.28	6.3×10^{-4}
5441	60296.7	60296.66	6.6×10^{-5}
6056	70702.8	70702.13	9.5×10^{-4}
6780	83550.3	83549.90	4.8×10^{-4}
7236	75369.6	75369.20	5.3×10^{-4}

Table 2. A comparison of several values of the second integral of B_y generated by the LabVIEW VI and the IDL routine. Note that the first column represents the index of elements in the two arrays.

From the similarity of the graphs of the integrals of B_y as well as the small relative errors shown in Table 1 and Table 2, we conclude that the new LabVIEW

VI corresponds well with the IDL Integration routine. The LabVIEW VI has a significant advantage in that it can be easily incorporated into larger projects, which are also written in LabVIEW, to analyze the measurement of magnetic field in superconducting undulators.

5 Future Plan

The authors have presented the development of a LabVIEW VI which generates the slope of electron trajectory, the position of electrons, and the slippage in a superconducting undulator. We plan to add other algebraic manipulations to this VI to generate other quality factors of an SCU, including K_{eff}, B_{eff}, and phase error.

6 Acknowledgement

1. This work is supported by U.S. Department of Energy, Office of Science, under Contract No. DE-AC02-06CH11357.
2. I would like to appreciate Matt Kasa for his mentorship throughout this project. I would also like to thank the Lee Teng Undergraduate Internship in Accelerator Science and Engineering and Argonne National Laboratory for providing this summer program in 2019.

Bibliography

[1] Clarke, J. (2004). *The Science and Technology of Undulators and Wigglers*. Oxford University Press, New York, 1 edition.

[2] Dejus, R. (2016). First and second integrals of magnetic field in an SCU. Argonne National Laboratory, Lemont, Illinois.

[3] Holst, B. (2005). Working of the undulator. Permission is granted to copy, distribute and/or modify this document under the terms of the GNU Free Documentation License.

[4] Kasa, M. et al. (2019). Design picture of an SCU. Argonne National Laboratory, Lemont, Illinois.

[5] Wolf, Z. (2004). Introduction to LCLS undulator tuning. pages 2–5.